Energy loss and scattering of energetic Sn ions interacting with H2: Prospects of Time-of-Flight investigations

University of Groningen

August 2021

rijksuniversiteit
groningen

Bachelor Research Project

Applied physics

Author:
F.Veen (S3397130)

Abstract

The innovation of semiconductor industries keeps minimizing the size of chips in technological devices, companies like ASML keep this innovation alive. The development of the extreme ultra violet light sources is pushing Moore's law forward, as the EUV light source can produce 13.5 nm light which makes the production of super small chips possible. In the EUV lithography machines of AMSL a multi-kilowatt laser hits tin droplets such that a plasma is created which emits the 13.5 nm light. However, highly energized tin ions are created as well which can damage the mirrors inside the light source. Hydrogen gas is used to slow down these ions, but this gas also absorbs part of the EUV light from the source. Therefore experiments are performed to investigate the interaction between tin ions and hydrogen gas, as the energy of tin ions passing through hydrogen gas can be measured by using time of flight spectroscopy techniques. The focus of this thesis will be to gain insight into the influence of energy straggling and range straggling on the time of flight of tin ions passing through a hydrogen target. To do so simulations based on the ARCNL ESA-ToF analyser set-up will be performed in the simulation program SRIM. Moreover, the prospect of using a localized pressure target will be investigated.

Contents

1 Introduction

In 1965 the American engineer Gordon Moore predicted that the number of transistors per silicon chip would double every year due to the increasing technological development. A decade later he revised his statement, as the rate of technological growth had slowed down. The new time frame became known as Moore's law: the number of transistors per chip doubles every two years.[1] Keeping this law alive is what drives the semiconductor industry to innovate. The challenge is taken by companies like ASML, who are the current leading company in building lithography devices for application in the semiconductor industry.

To keep up with Moore's law ASML has developed an extreme ultraviolet (EUV) light source, which uses light at a wavelength of 13.5 nanometers. The wavelength is the key to producing smaller transistors and thus increase the number of transistors per chip, as a smaller wavelength results in a better resolution. A sub 100 nm light source is therefore considered to be the current breakthrough in nano lithography. The light source is based on a laser produced plasma (LPP) in which a laser is focused on a stream of tin droplets. When this multi-kilowatt laser hits a tin droplet it will evaporate and be ionized such that a high-temperature plasma is created. This plasma mainly emits light in the EUV spectrum, this radiation then strikes a multilayered mirror which focuses the light into the lithography tool.[2] Even though the LPP source produces a spectrum of EUV light the wavelength of 13.5 nm is of key relevance, solemnly due to the relative high efficiency of multilayered MO/Si mirror at: 13.5 nm.

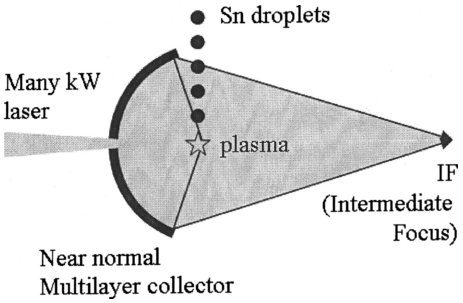

Figure 1: Schematic overview of a LPP source. A stream of tin droplets is hit by a high energy CO_2 laser and produces a hot plasma.[2]

Not only EUV light is produced by the tin plasma, as also high energy tin ions are produced. Due to their high energy the ions can damage nearby optic equipment, among which the very expensive multilayered mirror. To slow down these ions, and to mitigate other debris from the source, hydrogen (H_2) gas is used as buffer gas. A downside of using the hydrogen gas is the possibility that it absorbs a fraction of the EUV light from the source, which decreases the efficiency of the source. In this thesis the results of SRIM simulations will be discussed with the aim of establishing input for the design of future high-resolution experiments. The goal of these future experiments is to measure atomic scale energy transfer from Sn ions to H_2 molecules.

2 Theory

In this section the theoretical basis of time of flight simulations of tin particles traversing H_2 gas will be discussed. First of all the theory of the interaction between ions and matter and stopping power will be discussed. Then the concept of time of flight spectroscopy will be discussed to show how the time of flight relates to the energy loss of tins ions. At last the workings of SRIM will be discussed, while focusing mostly on the calculation of the projectile ion energy since it forms the basis of the time of flight calculations.

2.1 Stopping power

To slow down Sn ions a buffer gas can be used. The interaction of ions with gas cause the ions to lose energy and thus slow down. The amount of energy lost (dE) over a path length dx is quantified by the stopping power, defined as [3]

$$NS(E) = \frac{-dE}{dx}, \tag{1}$$

with S(E) the so called stopping cross section. The origin of energy loss lies in the interaction between the ion and atoms of the target. There are three mechanisms by which an ion can lose energy: nuclear energy loss, electronic energy loss and radiative energy loss. The energy loss due to elastic collisions between the nuclei of the target and the ion is referred to as nuclear energy loss. Energy loss due to inelastic collisions between bound electrons in the target and the ion is referred to as the electronic energy loss. At non-relativistic ion energies, which are the ion energies considered in this paper, the radiative energy loss can be neglected. The total stopping cross section is then the sum of the contributions of nuclear energy loss and electronic energy loss:

$$S(E) = S_n + S_e \tag{2}$$

2.1.1 Nuclear stopping

As mentioned before the stopping power is defined as the energy loss over a certain path length. Nuclear stopping is thus given by the energy loss due to different elastic collisions along a certain path. The classical description of elastic collisions between two particles can be used to find an expression for the reaction cross section. Reaction cross sections are used to theoretically describe average energy losses. The reaction cross section is a function of the energy transfer T from a projectile and its initial energy E, $\sigma(E, T)$. Momentum is conserved in an elastic collision such that the transfer of energy will depend on the scattering angle θ of the projectile atom. A schematic representation of the scattering variables, for both a laboratory and a center of mass coordinate system is given in figure 2.

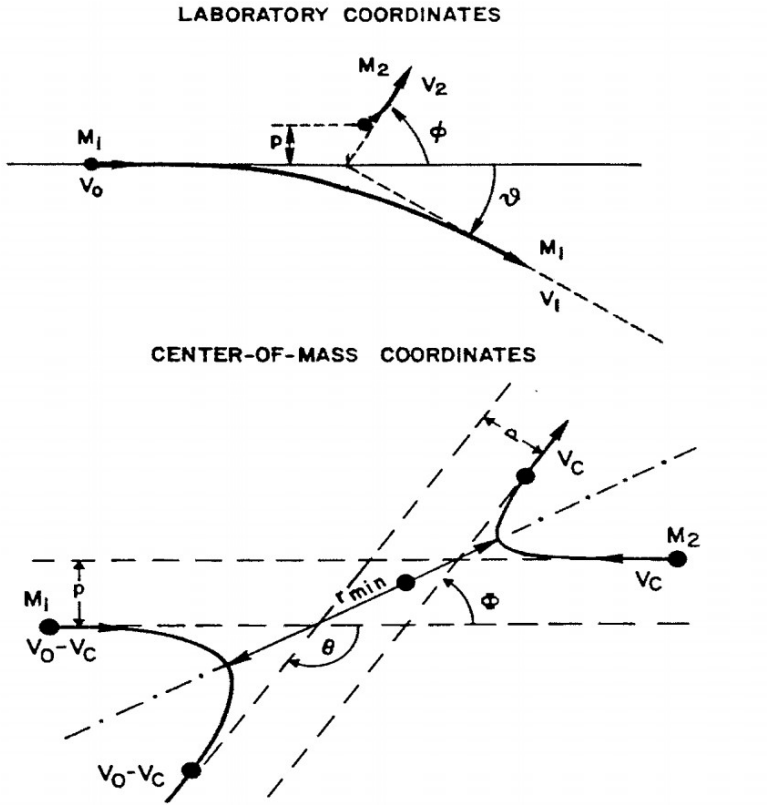

Figure 2: Schematic overview of the collision between a projectile and its target for a laboratory and a center of mass coordinate system. In this collision the projectile approaches from the left moving like a free particle. The projectile has mass M_1 and initial velocity V_0 and impact parameter p with the target particle. The final scattering angle from the projectile is given by θ in the laboratory frame and Θ in the CM frame, and the final projectile velocity by V_1. The target particle has mass M_2, recoil angle ϕ in the laboratory frame and Φ in the CM frame, and final velocity V_2. The upper figure shows a collision between projectile and target as seen from a laboratory frame, the bottom figure shows the same collision in a center of mass frame. The center of mass frame will be used to describe the mutual interaction of the two colliding particles by a force-field V(r), which only depends on the interatomic separation r. From [4]

For the center of mass coordinate system a system velocity can be defined such that there is zero net momentum in the system: [4]

$$V_C = \frac{M_1 V_0}{M_1 + M_2}. \tag{3}$$

The scattering and recoil angles of the laboratory and CM frame can be related through [4]

$$\Phi = \pi - \Theta = 2\phi, \tag{4}$$

such that the final velocity of the target can be derived to be [4]

$$V_2 = 2V_0 \frac{M_C}{M_2} \cos\phi, \tag{5}$$

where M_C is the center of mass energy. For an elastic collision the energy transfer as a function of the CM scattering angle can then be derived to be [4]

$$T = \frac{1}{2} M_2 V_2^2 = \frac{4E_0 M_1 M_2}{(M_1 + M_2)^2} \sin^2 \frac{\Theta}{2}. \tag{6}$$

Using the conservation of energy and angular momentum Lagrangian mechanics in polar coordinates can be applied to derive the complete scattering path in the CM frame, with Θ the azimuthal

polar coordinate and r the radial coordinate. The scattering angle θ along the complete scattering path can be derived to be [4]

$$\theta = \pi - 2\int_{r_{min}}^{\infty} \frac{pdr}{r^2[1 - \frac{V(r)}{E_c} - \frac{p^2}{r^2}]}, \tag{7}$$

where $E_c = E_0 m_2/(m_1 + m_2)$ is the center of mass energy, r is the radial polar coordinate from the projectile to the atom and p is the impact parameter as shown in figure. A more detailed description and complete derivation of the above mentioned equations can be found in [4]

The central force potential is determined by the interatomic forces between the two particles, which at small interatomic separations at high energies can be modelled by considering a screening function $\Phi(r)$ for the Coulomb potential such that [4]

$$V(r) = \frac{Z_1 Z_2 e^2}{4\pi\epsilon_0 r}\Phi(r/a), \tag{8}$$

where a is the screening length, which depends on the atomic numbers Z_1 and Z_2, and r/a the reduced radius (x). For modelling atomic collisions the ZBL potential is used, which is given by [4]

$$\Phi(x) = 0.1818e^{-3.2x} + 0.5099e^{-0.9423x} + 0.2802e^{-0.4028x} + 0.2817e^{-0.2016x} \tag{9}$$

and the screening length is given by

$$a = \frac{0.8854a_0}{Z_1^{0.23} + Z_2^{0.23}}. \tag{10}$$

The nuclear stopping power is the average energy transferred when summing over all impact parameters: [4]

$$S_n(E) = \int_0^{\infty} Td\sigma, \tag{11}$$

such that the nuclear stopping power can be calculated by using equations for the transferred energies and the scattering angle, which can be used for modelling ion trajectories in computer programs like SRIM.

2.1.2 Electronic stopping

Unlike for nuclear energy loss, the energy loss due to electronic stopping comes from inelastic collisions of the ion with the target. The term inelastic implies that kinetic energy is not conserved in collisions, as an collision between two particles can result in the excitation of bound electrons from the target or electrons from the electron cloud of the ion. The number of collisions of an ion with electrons is very high which severely complicates the description of all possible interactions, as the heavy ion can frequently change charge state while transversing the target medium. Therefore the electronic stopping power for heavy ions is usually given as simply function of the energy, which is an average taken over all energy loss processes for different charge states. As a consequence the SRIM predictions for heavy ions are significantly less accurate. [5]

Since the total stopping power is a combination of the electronic and nuclear stopping power it is important to know how much each one contributes to the total stopping power. The distribution between the nuclear and electronic stopping power is given in figure 3. From this figure the assumption can be made that the electronic stopping can be neglected in this paper, since at energies between 1-10 keV the contribution of the electronic stopping to the total stopping power is very small compared to the nuclear stopping.

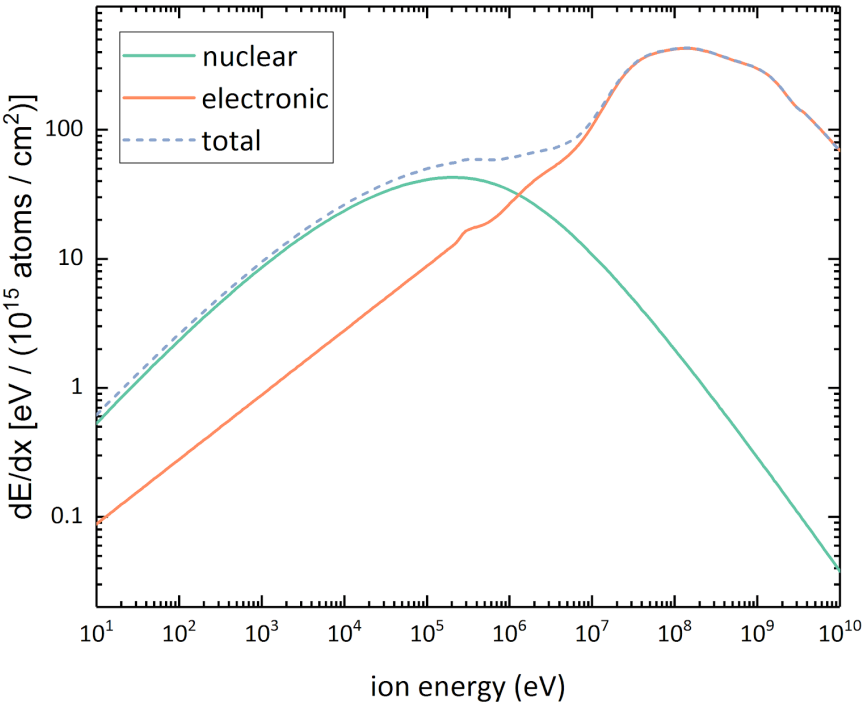

Figure 3: Electronic and nuclear stopping power contributions to the total stopping power for tin ions from laser-produced plasma. At ion energies between 1 keV and 10 keV the stopping power due to nuclear energy loss dominates. Values for nuclear and electronic stopping are obtained from tables in SRIM. [3]

2.2 Straggling

The expected path a charged particle can travel in a given medium before it comes to rest is referred to as the penetration depth. This projected range depends on the particles initial energy and the type of particle. However, when a particle transverses through matter statistical fluctuations occur in the number of collisions with the matter and the amount of energy lost in each of these collisions. An ion experiences a random amount of collisions at a random point along its path length. Therefore a number of identical particles starting out under identical conditions (with the same initial energy) will show a distribution of energies after transversing the matter to a certain depth. Moreover, these same statistical fluctuations cause the distribution of transversed path lengths before the particles come to a stop. This phenomenon of unequal energy losses under identical conditions is called energy straggling and the existence of different path lengths is called range straggling. [4]

2.3 Time of Flight spectroscopy

As mentioned in section 2.1, to quantify the energy loss of tin ions hitting a gas target of a certain thickness at particle concentration n the stopping-cross section is introduced. This stopping cross-section cannot be measured directly, but with the help of time of flight measurements it can be calculated. In a laser produced plasma not all ions which are created will have the same initial energy. Therefore a method is developed in which the ion energy is selected at the end of a tube, where the time of flight is measured as well. The ions fly through a tube of a certain length (L), with a non constant gas pressure. All energy of the ion is considered to be kinetic energy. The ion travels along a trajectory with a density of n(x), and arrives at the end of the tube with end energy E. The initial energy is denoted by E_0, such that the energy loss is given by[6]

$$\Delta E(x) = E_0 - E(x), \tag{12}$$

combining this equation with the previous gives

$$\Delta E(x) = \int_0^x n(x')S(E(x'))\,dx'. \tag{13}$$

Using the derivations from Abramenko et al. (2018) this equation can be rewritten in terms of measurable quantities, such that the stopping cross-section for a uniform pressure distribution is given by

$$S(E) = -\frac{4EkT}{p_{eff}L}\frac{\Delta t}{t_{vac}}. \tag{14}$$

In this equation k and T respectively represent the Boltzmann constant and the gas temperature. The $p_{eff} = \overline{p}\eta$, where η characterizes the non-uniformity of gas distribution in the tube and $\overline{p}$ is the average gas pressure in the tube. The total time of flight is given by t = δt + t_{vac} and t_{vac} represents the time of flight of a tin ion with energy E in a tube without gas and is given by [6]

$$t_{vac} = L/\sqrt{2E/m}. \tag{15}$$

In time of flight spectroscopy experiments the density of gas will be changed, by measuring the according time of flight the influence of the pressure distribution on the stopping power of the buffer gas can be determined.

2.4 The Stopping and Range of Ions in Matter (SRIM)

The computational program used for performing the simulations of tin ions transversing through hydrogen gas is called SRIM. This program is a convenient tool to approximate the path length and energy of low energy ions. The SRIM program is based on the binary collision approximation, which is widely used in computer simulations of the interactions of energetic atoms with solid targets. [5] The assumption on which the binary collision approximation is based is that all interactions of energetic atoms can be separated into a series of two-body encounters. The theory of nuclear and electronic stopping in section 3.1 covers these two-body collisions.

The structure of the target atoms in the model greatly impacts the outcome of the simulations. The SRIM model is based on the class of BCA models known as the Monte Carlo codes. In these models the target is structure less which means that the impact parameters, flight distance, mean free path, scattering angles and other parameters are all generated randomly from a probability distribution over a given domain. [5] There is no correlation between the target atoms except for the location restrictions determined by the density of the target. To evaluate the atomic scattering SRIM uses an analytic formula to determine, among others, the parameters mentioned above. This formula quickly calculates the scattering angle of an ion, unlike formula 5, and is called the Magic formula. The Magic formula allows for a quick solution to the scattering problem with a high precision. [4] [7]

2.5 Time of Flight calculations with SRIM

To get the simulated distribution of the time of flight as a function of the energy the output files of SRIM are analyzed with the help of MATLAB scripts. The basis of this script comes from the equation given for the kinetic energy of the projectile ion, equation:

$$E_k = \frac{1}{2}mv^2, \tag{16}$$

where E_k is the kinetic energy,m is the mass of the ion and v is the velocity of the ion. Combining the previous equation with the equation for traveled distance with constant velocity

$$d = vt, \tag{17}$$

where t is the time of flight and d is the path length, gives the final equation for the time of flight as

$$t = \frac{d}{\sqrt{\frac{2E_k}{m}}}. \tag{18}$$

The MATLAB script is constructed in such a way that it separately calculates the time of flight after each collision. In this way the kinetic energy of the ion is given by the energy of the ion after each collision, and the path till the next collision is assumed to be travelled at a constant velocity. This approximation is supported by the localized contributions of nuclear and electronic stopping. As the nuclear stopping is much higher than the electronic stopping at the energies which are considered in this thesis, it is safe to assume that the ion travels at constant velocity between collisions as the deceleration of the ions due to electron stopping will be only small.

3 Experimental Set-up

The focus of this thesis is to estimate the effects of energy straggling and range straggling on the time of flight for the ARCNL (Advanced Research Center for Nanolithography) ESA-Tof analyser. From the definitions given in section 2.2 one would expect a spread in time of flight due to the combination of energy straggling and range straggling. The hypothesis is that the fluctuations in the amount of energy lost during each collision together with the fluctuations in flight path will lead to a spread in time of flight for ions which have the same final energy. In this section the experimental set-up of this analyser will be addressed and the parts of this set-up which are relevant to this thesis will be briefly introduced.

3.1 ARCNL ESA-Tof analyser

A schemtic overview of the set-up is given below:

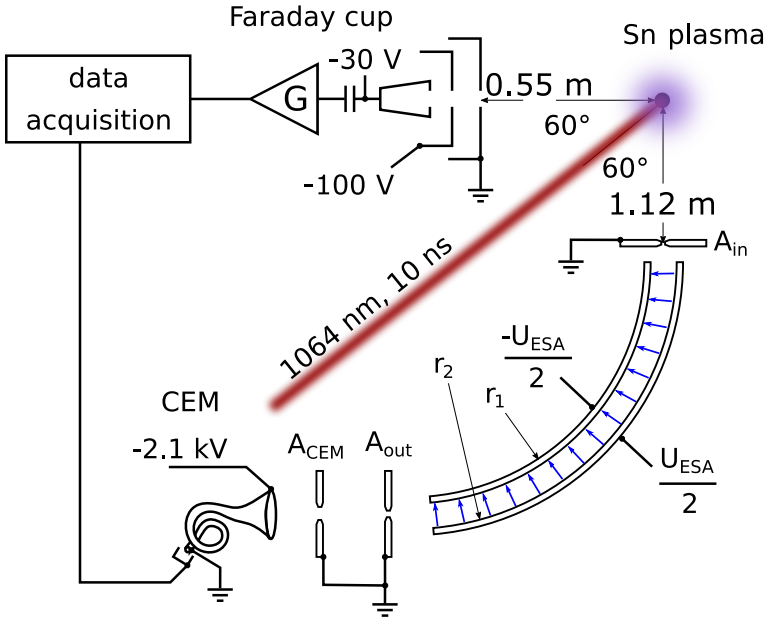

Figure 4: Schematic overview of the ARCNL set-up. From the laser produced plasma (LPP) source the ions travel through a tube with hydrogen gas with a length of 1.12 m. A selection takes place at the electrostatic analyser (ESA), where only ions of a certain energy are able to pass through. After passing through the ESA the time of flight is measured at the CEM detector. [8]

The energetic ions originate from a laser produced plasma (LPP) and firstly encounter a flight path of 1.12m. This path can be filled with H_2 gass such that the hydrogen atoms can interact with energetic tin ions (and thus slow them down). Then the (slightly less) energetic ions will reach the electrostatic analyser (ESA), which is designed to filter the ions according to their corresponding energy. The pass energy for the ESA filter depends on the charge of the ion and the ion energy. The pass energy is given by

$$E_{pass} = U_{ESA} 5q, \tag{19}$$

with q the charge of the ion and U_{ESA} the voltage of the ESA analyser. This voltage can be adjusted, such that for each value of q only ions with a specific kinetic energy will be able to pass through the ESA, other ions will be filtered out. In this way all ions which have passed through the ESA will have the same amount of energy for each value of q. These ions will travel further to the CEM detector where the total time of flight will be measured. [8]

3.2 SRIM Simulations

To perform simulations of the interactions of hydrogen atoms with tin ions the program SRIM, in which the interaction of ions with matter can be simulated, will be used. The calculations

which produce the corresponding results are explained in the theory section and a more detailed description can be found in ref [4].

The SRIM settings for the simulations of the ARCNL ESA analyser set-up can be found in the table and figure below, these settings are implicitly stated in order to be able to reproduce the simulations.

TRIM setup	Setting
Type of TRIM Calculation	
Damage	Ion Distribution and Quick Calculation of Damage
Basic Plots	NO Graphics
Ion data	
Symbol	Sn
Name of Element	Tin
Atomic Number	50
Mass (amu)	119.902
Energy (keV)	1/3/10
Angle of Incidence	0
Target Layer	
Layer Name	Hydrogen
Width (μm)	112/336/672/1120
Density (g/cm^3)	9×10^{-8}
Compound Correction	1.3550
Gas	✓
Input Elements to Layer	
Symbol	H
Name	hydrogen
Atomic Number	1
Atom Stoich	1
Displacement energy (eV)	0.1
Lateral	3
Surface	2
Special Parameters	
Name of Calculation	Sn(10) into hydrogen
AutoSave at Ion	10000
Total number of Ions	99999
Random Numer Seed	
Stopping Power Version	SRIM-2008
Plotting Window Depths Min	0 Å
Plotting Window Depths Max	$1.12 \times 10^6/3.36 \times 10^6/6.72 \times 10^6/11.2 \times 10^6$ Å
Output Disk Files	
Ion Ranges	✓
Transmitted Ions/Recoils	✓
Collision Details	✓

Table 1: SRIM simulation settings

3.2.1 SRIM Settings

The program SRIM allows for different calculations to be made. Therefore it is important to discuss which settings have been chosen. In the first interface menu of SRIM there are several options to be selected (see figure 5). For this experiment the type of damage calculation will be set to "Ion Distribution and Quick Calculation of Damage" with No graphics. This calculation mode has been chosen because of the type of experiment: the goal is to calculate the time of flight of tin ions, thus the ion distribution is the most important information. Moreover, the damage of target will be only minimal due to the fact that the target is a gas.[7]

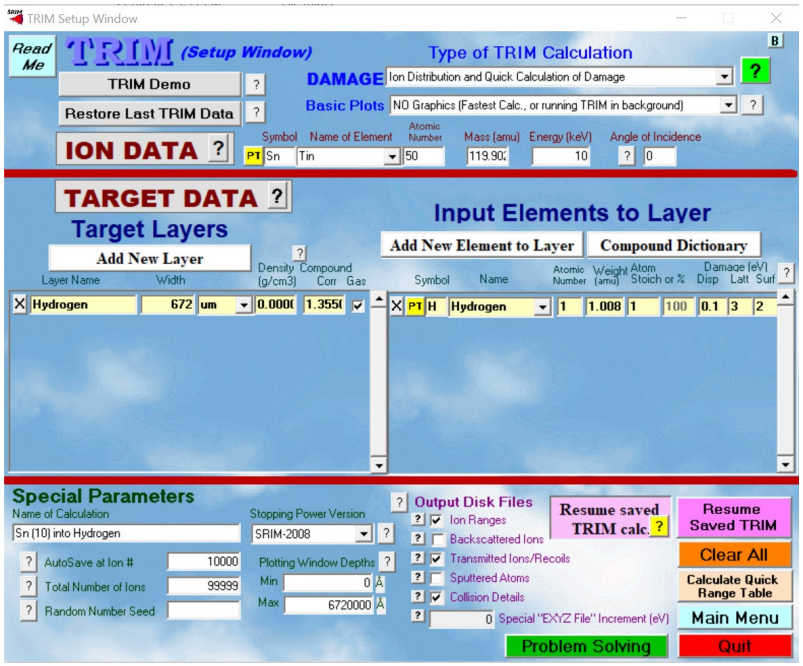

Figure 5: The SRIM interface where adjustments to the simulation settings can be made, the settings used for this experiment are implicitly stated in table 1 and explained in section 4.2.1

The next few settings under Ion data in table 1 are straightforward. A tin ion of mass 119.902 is selected for the ion beam, with starting energy of 1/3/10 keV. Since our beam of ions should be aimed straight at the hydrogen target the angle of incidence is 0. Then for the target layer hydrogen is selected. Since the goal is to simulate hydrogen gas at a pressure of 1×10^{-4} mbar - 1×10^{-3} mbar one has to accordingly adjust the density and length of the target, as there is no option to adjust the pressure in SRIM. According to the research from K. Bijlsma (2020) [9] it is possible to simulate gas targets at low pressure by using lower densities and smaller target lengths. The standard pressure in SRIM is 1 bar (atomic pressure) with an according density for hydrogen gas of 8.99×10^{-5} cm^3/g . To decrease the pressure to match the pressure in the ARCNL set-up at first it is possible to decrease the density to 8.99×10^{-8}, which is the limit in SRIM. When decreasing the density even more an error will occur in SRIM. To decrease the pressure for the remaining orders of magnitude the target length will be decreased. The idea is based on the the fact that a target with length L and density n contains as many atoms as a target with length L/3 and denisty 3n. Therefore, when decreasing the length of the target by a certain factor the density will decrease with the same factor. Thus to simulate a target of 1.12 m at 1×10^{-4} mbar one needs to set the density at 8.99×10^{-8} and adjust the target length to 112 μm.

Next, the gas correction and gas compound will be discussed, due to their influence on the SRIM calculations. The behaviour of gases and solids in their respective structures is different such that a correction is needed for a gas target in comparison to a solid target. In a solid phase the ion-target interaction is strongly influenced by the screening of the intruder (ion) charge by the electron cloud formed from conduction electrons. Due to this phenomena more collisions will appear in a solid phase which then influences the stopping power of the target. In a gas phase the interaction is determined by the interatomic potential between the ion and target and depends on the atomic charges and the states of the electrons which are bound to the ion. Moreover, the ion will interact with the other target atoms quite quickly which means the excitation of the ion's own electrons may not relax before the next collision resulting in a local target electron density around the ion. In a gas phase the electron density is lower which means the interaction of ions and electrons will be lower. However, the increase in local electron density will decrease interactions of the ion with distant target atoms, which then lowers the ion target interaction in solids compared to gasses. From these three effects the third one has the most influence on the ion-target interaction and thus the stopping power in gasses is usually higher than in solids for low velocity ions (below 2 MeV/u). [4] [10]

The second correction factor, the compound correction, is a result of the large effect of atomic bonds on the stopping power. In SRIM the Core and Bond (CAB) approach is used to generate corrections. The CAB approach suggests that the stopping power in compounds can be represented by the superposition of stopping by the different atomic cores and adding the stopping due to the bonding electrons. The contribution of the core atom is determined by using Bragg's rule of linearly adding the stopping from each atom in the compound. The contribution of the chemical bonds to the stopping power is represented by the correction factor , which is dependent on the chemical nature of the bond and thus varies for different bonds. Thus the value found in table 1 corresponds to the correction factor for a hydrogen bond. [4] [11]

When adding the Target layer to the Input element to Layer the option of setting the displacement energy is critical. The displacement energy is defined as the energy needed for a recoil atom to overcome the target's lattice forces and move away more than one atomic spacing from the lattice structure.[4] SRIM only shows collision data of collisions with a higher energy value than this displacement energy. However, as the simulation will use a gas target there is in fact no lattice structure so in theory the displacement energy should be zero. This is not a possible input value in SRIM thus this value is set to the lowest value possible (0.1 eV). Since the time of flight calculations depend strongly on the collision data it is important to collect as much collision data as possible since it will improve the quality of the corresponding results.

3.2.2 Approximations

After running the simulations through SRIM the data will be analysed such that a ToF calculation can be made. To make these calculations possible some assumptions will have to be made. First of all, all ions are assumed to travel in a straight line from the start of the ion beam to the end of the flight path. This assumption is made because of the great difference in mass between the light hydrogen atom and the heavy tin ion.[3] When a collision occurs the scattering angle will be almost zero, which can be confirmed by looking at the collision data. Moreover, it is assumed that the ion will travel with a constant velocity between each collision, as mentioned and explained before in the theory section. After the flight path of 1.12 m with hydrogen gas it is assumed that no energy loss occurs in the remaining free flight path of 0.35m in the ESA-analyser before the ion reaches the CEM detector.

4 Results and Discussion

In this section the results of the previously introduced simulations will be given and discussed. First the results of the uniform pressure distribution simulations will be discussed. Then the results of a localized pressure distribution will be presented and the prospects of such a distribution will be discussed.

4.1 Uniform pressure distribution

In this section the results of the uniform pressure distributions are presented in the form of scatter plots of final ion energy and their time of flight, and in the form of a histogram of the time of flight. The previously introduced simulations are performed at three values for the initial ion energy (1,3,10 keV) and for four different pressures (1×10^{-4} mbar, 3×10^{-4} mbar, 6×10^{-4} mbar, 1×10^{-3} mbar). In the figures below the results of these simulations are presented in the form of a scatter plot of time of flight as a function of the ion energy at the CEM detector (E_{cem})

4.1.1 ToF for 1 keV tin ions

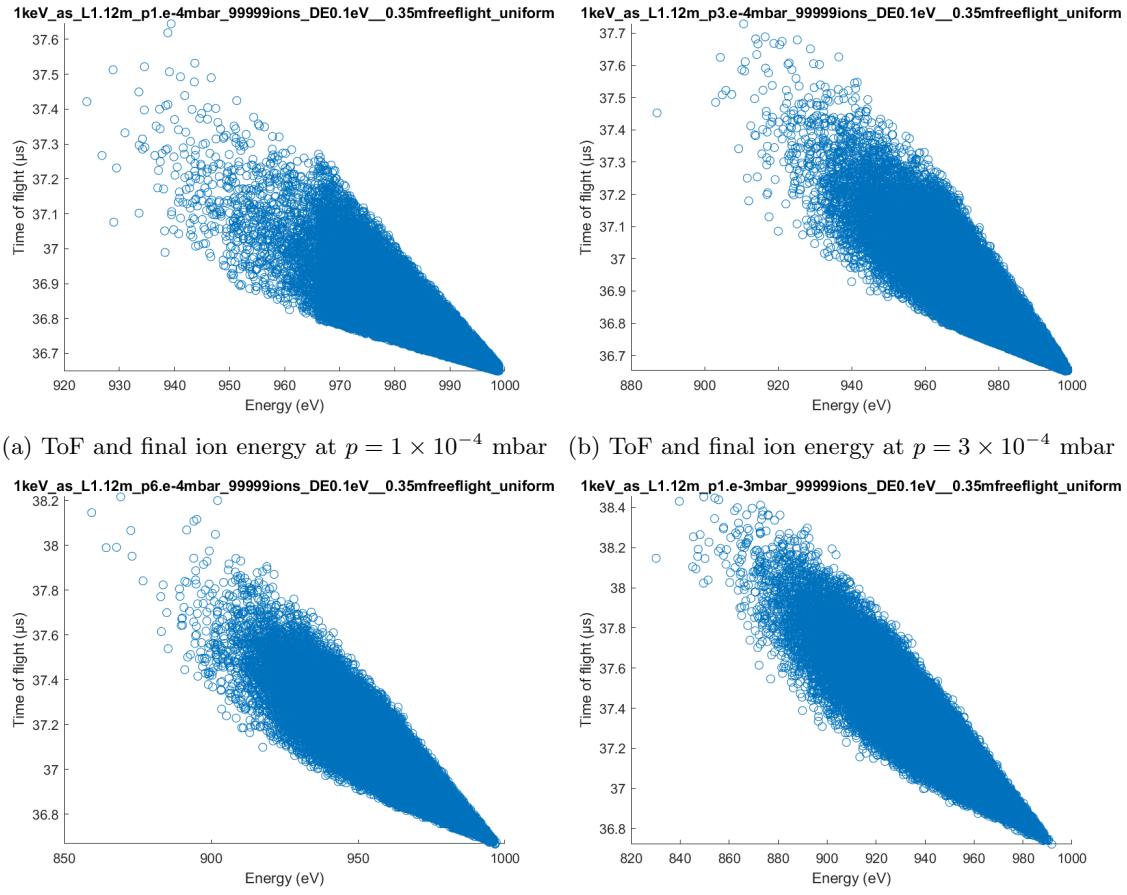

(a) ToF and final ion energy at $p = 1 \times 10^{-4}$ mbar (b) ToF and final ion energy at $p = 3 \times 10^{-4}$ mbar

(c) ToF and final ion energy at $p = 6 \times 10^{-4}$ mbar (d) ToF and final ion energy at $p = 1 \times 10^{-3}$ mbar

Figure 6: The simulated time of flight and final energies (ion energy at L=1.47m) for tin ions with an initial energy of 1 keV (ion energy at L=0). The vertical axis gives the time of flight of an ion, with on the horizontal axis their corresponding final energy. For each simulation a total of 99999 ions are simulated. Please note the difference in axes scaling of figures a,b,c,d.

From the figures above a few important observations can be made. First of all, one can see that for all pressure distributions there is a spread in time of flight for ions which have the same value of final energy E_{CEM}. The spread in time of flight becomes larger as the value of E_{CEM} decreases.

Both observations can be explained by the previously introduced theory. The spread in time of flight is a result of energy straggling and range straggling. As mentioned before the ions lose the largest part of their energy by colliding with a hydrogen atom. These collisions can happen at any location in the tube, as there is an uniform pressure distribution. When ions hit a hydrogen atom at the beginning of the tube they will travel the remainder of the distance with a lower velocity, due to their lower energy. Ions which have a lower value of E will be influenced more by the described process of random collisions. Therefore as the final energy E decreases the spread in time of flight will become larger, which is why the energy scatter plots in figure 6 have a cone like shape. From figure 6 one can see that the spread in time of flight as a result of the energy straggling and range straggling reaches a value between 0-1 μs.

Different pressures were simulated to investigate how the pressure would effect the spread in time of flight. From the above figures one can see that as the pressure increases in general the spread in time of flight increases as well. This observation can be explained by the fact that at a higher pressure level more atoms are present which can collide with the ions, which will essentially increase the energy straggling and range straggling and thus increase the spread in time of flight. This increasing spread in time of flight becomes more visible in the time of flight histograms in figure 7 below. One can see that as the pressure increases the peak intensity decreases because the peak broadens. Moreover, the peak position shifts to the right, mostly explained by the increasing stopping power of the target as the pressure increases.

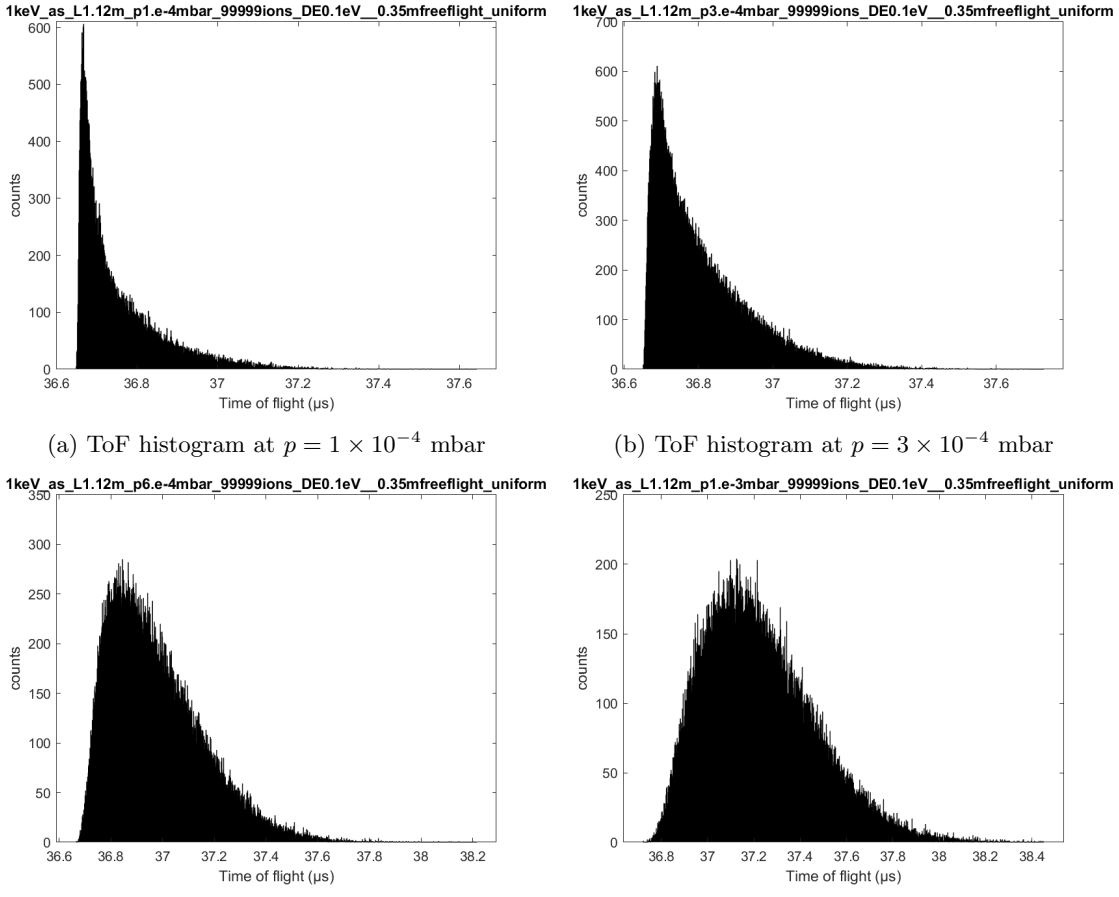

(a) ToF histogram at $p = 1 \times 10^{-4}$ mbar

(b) ToF histogram at $p = 3 \times 10^{-4}$ mbar

(c) ToF histogram at $p = 6 \times 10^{-3}$ mbar

(d) ToF histogram at $p = 1 \times 10^{-3}$ mbar

Figure 7: The figures a,b,c and d show the histogram of the simulated time of flight, with a bin size of 1 nanosecond. All Sn ions have the same initial energy (at L=0) of 1 keV. Please note the difference in axes scaling of figures a,b,c,d.

4.1.2 ToF for 3 keV and 10 keV tin ions

The same simulations as for 1 keV tin ions were performed for ions with an initial energy of 3 keV and 10 keV, to observe how the increase in initial energy would affect the spread in time of flight. In figures 8 and 9 the results of the time of flight as a function of the final energy E_{CEM} are presented in a scatter plot.

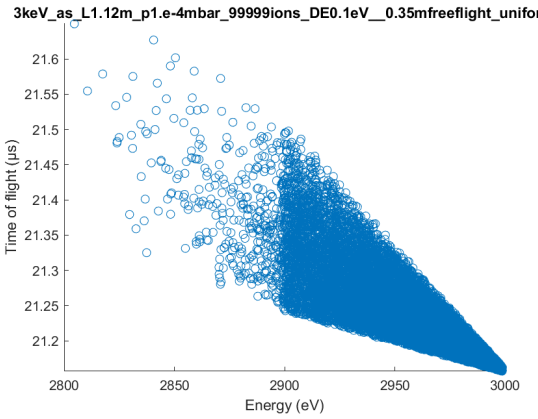

(a) ToF and final ion energy at $p = 1 \times 10^{-4}$ mbar

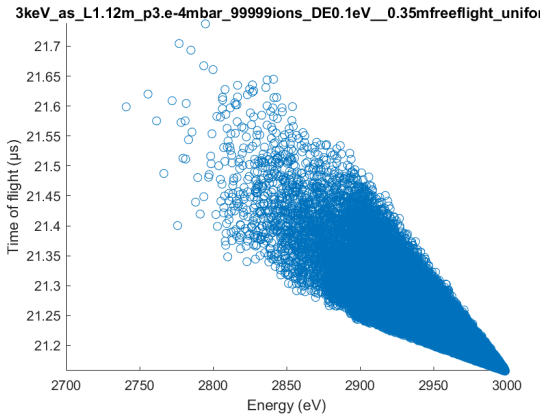

(b) ToF and final ion energy at $p = 3 \times 10^{-4}$ mbar

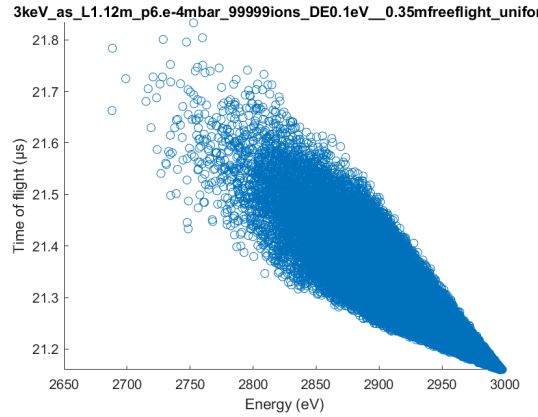

(c) ToF and final ion energy at $p = 6 \times 10^{-4}$ mbar

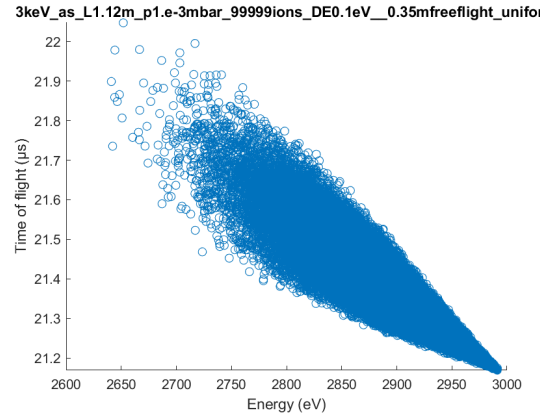

(d) ToF and final ion energy at $p = 1 \times 10^{-3}$ mbar

Figure 8: The simulated time of flight and final energies (ion energy at L=1.47m) for tin ions with an initial energy of 3 keV (ion energy at L=0). The vertical axis gives the time of flight of an ion, with on the horizontal axis their corresponding final energy. For each simulation a total of 99999 ions are simulated.Please note the difference in axes scaling of figures a,b,c,d.

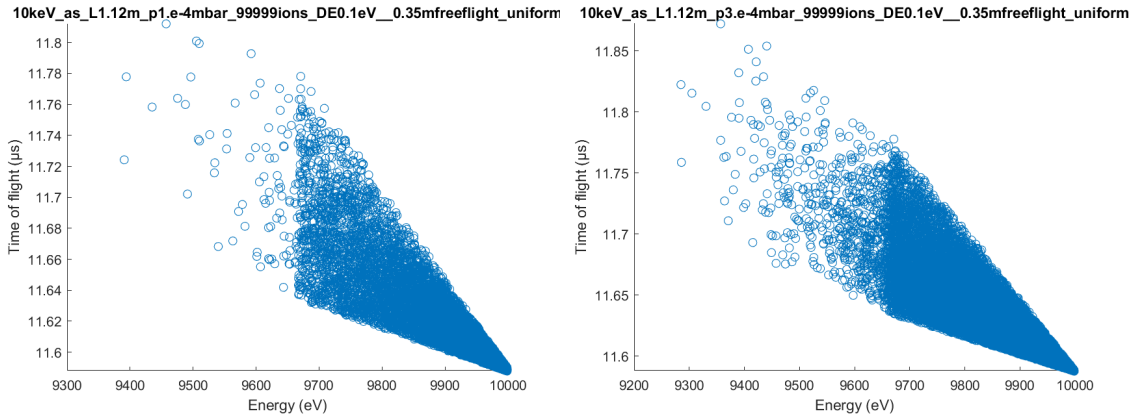

(a) ToF and final ion energy at $p = 1 \times 10^{-4}$ mbar (b) ToF and final ion energy at $p = 3 \times 10^{-4}$ mbar

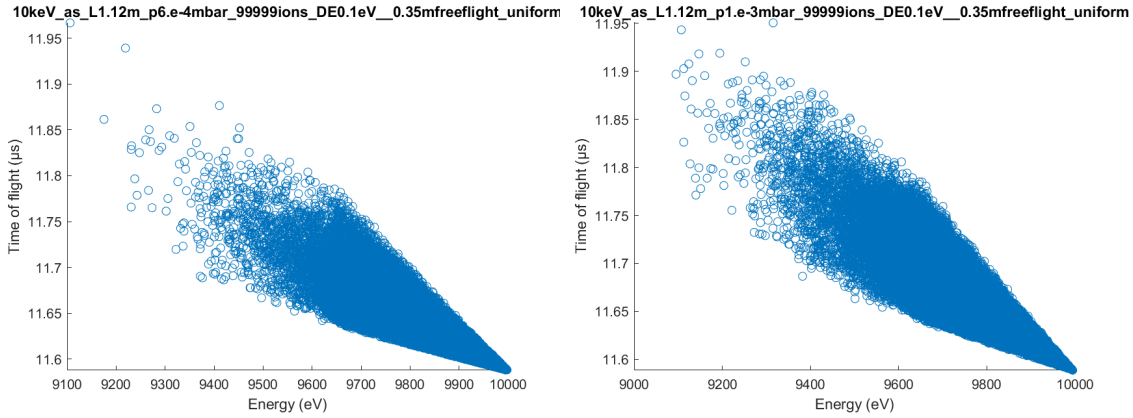

(c) ToF and final ion energy at $p = 6 \times 10^{-4}$ mbar (d) ToF and final ion energy at $p = 1 \times 10^{-3}$ mbar

Figure 9: The simulated time of flight and final energies (ion energy at L=1.47m) for tin ions with an initial energy of 10 keV (ion energy at L=0). The vertical axis gives the time of flight of an ion, with on the horizontal axis their corresponding final energy. For each simulation a total of 99999 ions are simulated.Please note the difference in axes scaling of figures a,b,c,d.

From figures 8 and 9 one can make a similar observation as for the scatter plots in figure 6, as the final energy of the ions decreases the spread in time of flight becomes larger. Also, like in figure 6, the spread in time of flight becomes larger as the pressure of increases. In absolute values the spread in ToF does becomes smaller as the energy of the ions increase, but this is a result of the ions having a higher average energy and thus a higher average velocity. In figures 10 and 11 the time of flight histograms for 3 keV and 10 keV ions are presented.

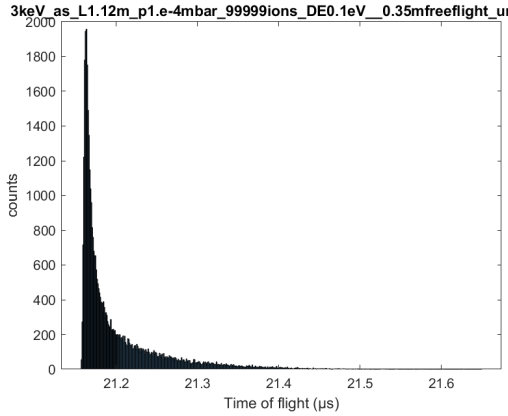

(a) ToF histogram at $p = 1 \times 10^{-4}$ mbar

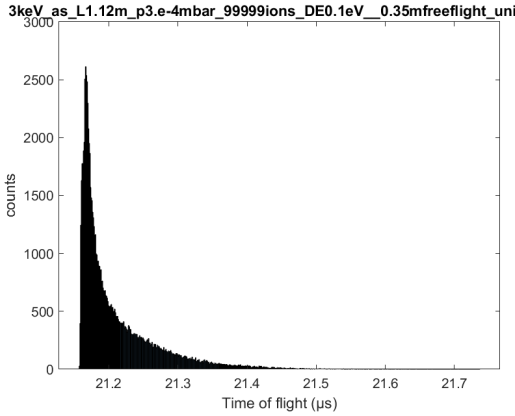

(b) ToF histogram at $p = 3 \times 10^{-4}$ mbar

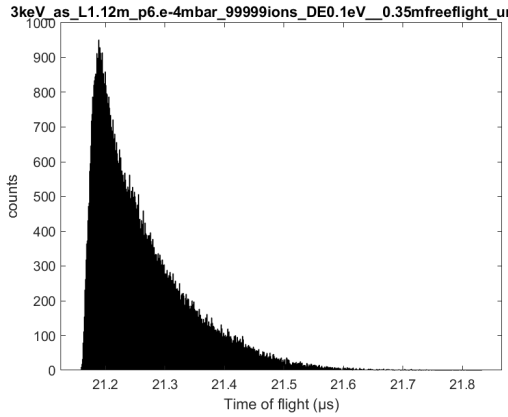

(c) ToF histogram at $p = 6 \times 10^{-3}$ mbar

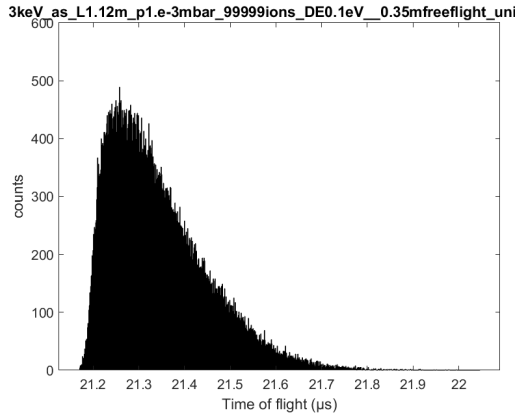

(d) ToF histogram at $p = 1 \times 10^{-3}$ mbar

Figure 10: The figures a,b,c and d show the histogram of the simulated time of flight, with a bin size of 1 nanosecond. All Sn ions have the same initial energy (at L=0) of 3 keV.Please note the difference in axes scaling of figures a,b,c,d.

As with the 1 keV ions the ToF histogram of the 3 and 10 keV ions show a shift of the peak position to the right as the pressure increases. Moreover, the maximum number of counts at the peak position decreases as the pressure increases for 3 keV and 10 keV, as with the 1 keV ions. Interesting to note is that the number of counts is a lot higher for the 3 keV and 10 keV ions, compared to the 1 keV ions. However, this can be explained by noting that the same bin size is used for the histograms of all different energies. Obviously when the average energy of the ions increases the ToF decreases so more ions will be 'caught' within one nanosecond. The decision to use the same bin size for every histogram was made because the 1 nanosecond bin size best represented the registration time of the CEM detector. For the same reasons as mentioned above the spread in ToF is smaller in higher energy ions.

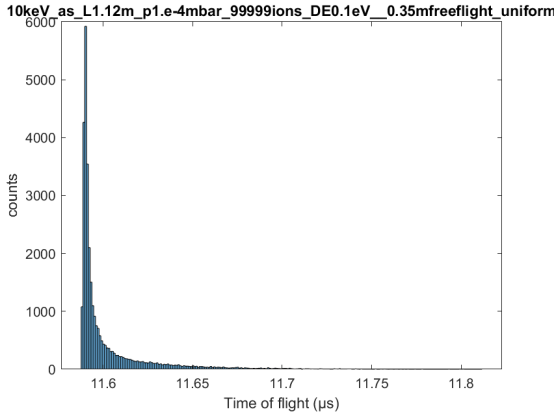

(a) ToF histogram at $p = 1 \times 10^{-4}$ mbar

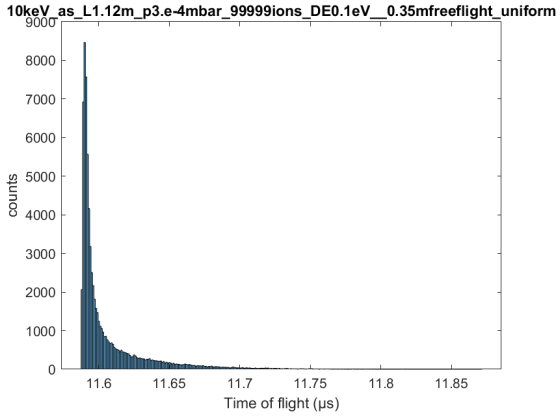

(b) ToF histogram at $p = 3 \times 10^{-4}$ mbar

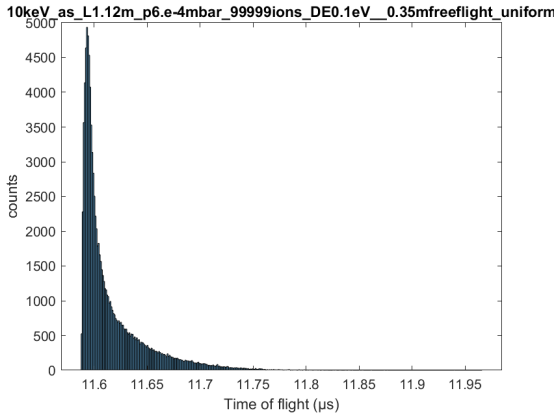

(c) ToF histogram at $p = 6 \times 10^{-3}$ mbar

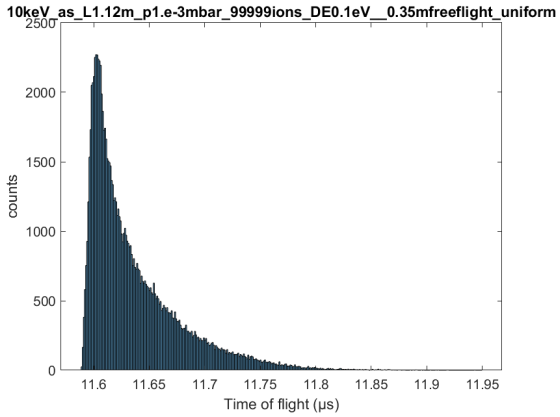

(d) ToF histogram at $p = 1 \times 10^{-3}$ mbar

Figure 11: The figures a,b,c and d show the histogram of the simulated time of flight, with a bin size of 1 nanosecond. All Sn ions have the same initial energy (at L=0) of 10 keV. Please note the difference in axes scaling of figures a,b,c,d.

4.1.3 Discussion of the uniform pressure distribution simulations

The results of the performed simulations presented in this section show that the spread in ToF due to energy straggling and range straggling is significant enough to possible influence the quality of a recorded ToF spectrum from the ARCNL ToF set-up. The scatter plots and histograms could have been analysed with more statistics but due to the fact that this experiment was done mostly to investigate the prospects and possible influence of energy straggling and range straggling on the ToF an extra statistical analyses would not have contributed much to eventual results, as this experiment still consists of mostly simulations and no definite results. It is difficult to make a direct comparison between these simulations and experimental data, unlike the experimental results the ToF histograms in figures 7, 10 and 11 do not have an energy selection (E_{CEM} is not the same for all ions).

4.2 Localized pressure distribution

To limit the influence of energy straggling and range straggling on the ToF a different simulation was performed to investigate if a hypothetical localized pressure distribution could reduce the spread in ToF. The simulations were performed in a similar way to the simulations for the uniform pressure distribution. However, to simulate a localized pressure distribution it was assumed that the hydrogen gas only interacted with the tin ions in a small path length of 1 cm located at 0.555 m from the ion source (halfway of the 1.12 m tube). Then after this 1 cm interaction path the ions were assumed to travel the remainder of the path with their final energy after the 1 cm interaction space.

Therefore the SRIM simulations for a localized prressure target were performed at a target depth of 1 μm and density 9×10^{-5} to simulate a target of 1 cm at a pressure of 1.12×10^{-1} mbar, which was chosen to ensure that as many target atoms are present in the localized target of 1 cm as there are atoms in the uniform pressure target of 1.12m at a pressure of 1×10^{-3} mbar. Moreover, the MATLAB script was adjusted to fit the new localized pressure distribution. These simulations were performed for three different values of initial energy, the same as in previous simulations. The results of these simulations are presented in the form of scatter plots of the time of flight as a function of the final energy and histograms of the time of flight in figure 12.

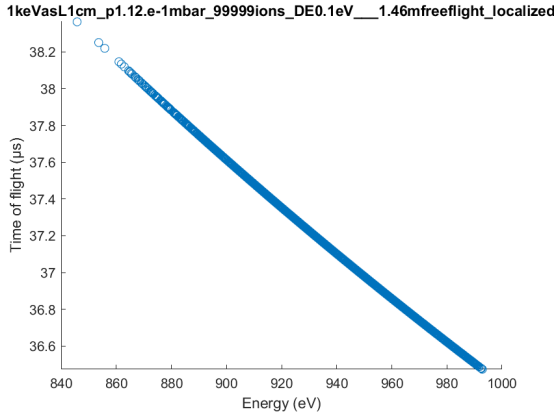

(a) ToF and final ion energy for 1 keV ions

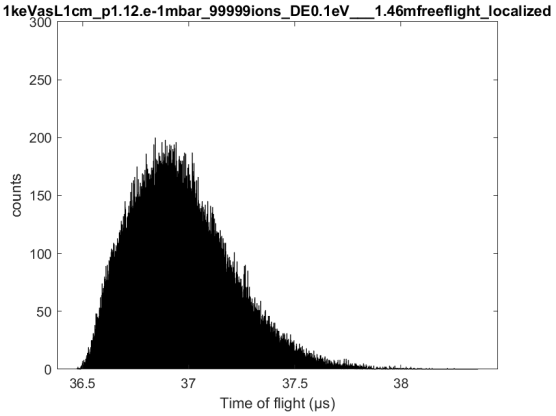

(b) ToF histogram for 1 keV ions

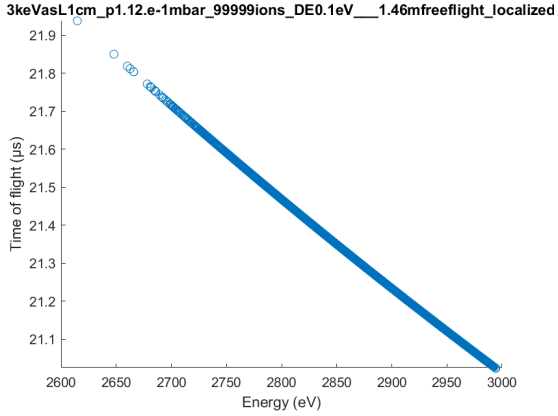

(c) ToF and final ion energy for 3 keV ions

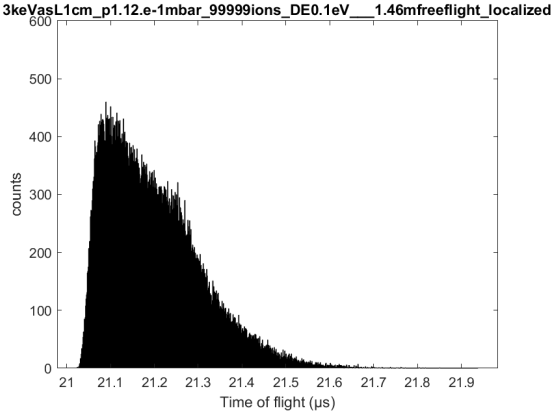

(d) ToF histogram for 3 keV ions

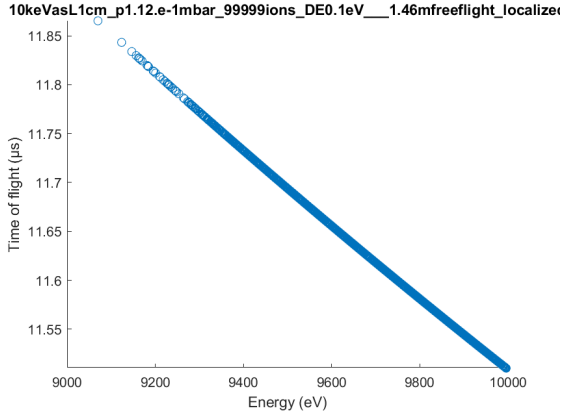

(e) ToF and final ion energy for 10 keV ions

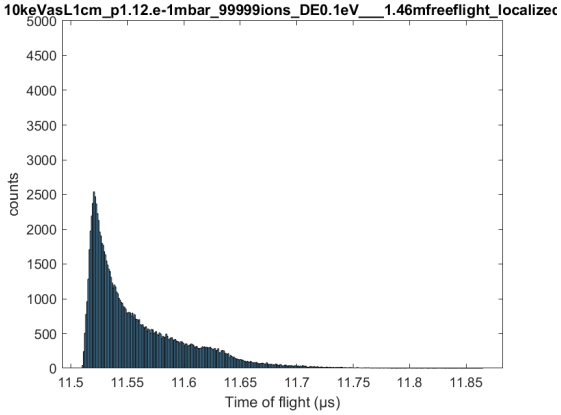

(f) ToF histogram for 10 keV ions

Figure 12: The figures a,c and e show the simulated time of flight and final energies (ion energy at L=1.47m) for tin ions with an initial energy of 1/3/10 keV (ion energy at L=0) for a localized pressure distribution at p = 1.12×10^{-1} mbar. The vertical axis gives the time of flight of an ion, with on the horizontal axis their corresponding final energy. For each simulation a total of 99999 ions are simulated. Figures b,d,f show the histogram of the simulated time of flight for a localized pressure distribution p = 1.12×10^{-1} mbar, with a bin size of 1 nanosecond.Please note the difference in y-axis scale in figures b,d,f.

4.2.1 Discussion localized pressure target

In the figures 12 a,c,e one can see that a localized pressure target of 1 cm greatly reduces the spread in ToF. as can be expected since the localized target almost eliminated the energy straggling and

range straggling. Therefore the localized pressure target shows good perspective for the ARCNL set-up. The histograms in figures 12 b,d,f do not give relevant information for the ARCNL set-up since there is no energy selection in this simulation while there is an energy selection in the ARCNL ToF-ESA set-up.

5 Conclusions

The results from the uniform pressure target simulations show that there is a significant influence of energy straggling and range straggling on the ToF of tin ions. The resulting spread in ToF will influence the quality and readability of the ToF spectra recorded in the ARCNL set-up. To eliminate the influence of energy straggling and range straggling a localized pressure distribution is suggested. This localized pressure target shows good potential, but will present a new challenge of being able to implement a localized pressure target in the set-up, which is challenging. However, the accuracy of these simulations depends largely on the accuracy of SRIM, which limits this research method. To achieve more detailed and accurate results experimental data is needed to be able to compare the results to the simulated results. However, the method and results presented in this thesis are not yet suitable for such a direct comparison, due to the earlier mentioned lack of energy selection in the scatter plots and ToF histograms. For further research one could improve the simulations such that an energy selection like in the ESA is possible, such that the simulations can be compared directly to experimental data.

References

[1] Britannica. *Moore's law*. Dec. 2019. URL: https://www.britannica.com/technology/Moores-law.

[2] Jos Benschop et al. "Extreme ultraviolet lithography: Status and prospects". In: *Journal of Vacuum Science and Technology B: Microelectronics and Nanometer Structures Processing,Measurement, and Phenomena* 26.2204 (2008).

[3] R. Hoekstra. *Power Point: StoppingThingies*. 2020.

[4] J.F. Ziegler, J. Biersack, and U. Littmark. *The Stopping and Range of Ions in Matter*. Pergamon Press, 1985.

[5] Mark T. Robinson and Ian M. Torrens. "Computer simulation of atomic-displacement cascades in solids in the binary-collision approximation". In: *PHYSICAL REVIEW B* 9.12 (1974).

[6] D.B. Abramenko et al. "Measurements of hydrogen gas stopping efficiency for tin ions from laser-produced plasma". In: *Applied Physics Letters* 112.164102 (2018).

[7] Jean-Paul Crocombette and Christian Van Wambeke. "Quick calculation of damage for ion irradiation: implementation in Iradina and comparisons to SRIM". In: *EPJ Nuclear Sci. Technol.* 5.7 (2019).

[8] L. Poirier et al. "Absolute cross-calibration of a combined electrostatic and Time of Flight analyzer for energy- and charge-state-resolved spectrometry of tin laser-produced plasma". 2020.

[9] K. Bijlsma. *Simulate target gases of low pressure with SRIM*. Sept. 2020.

[10] M. Bergsmann et al. "Phase effect in stopping of H ions in Mg". In: *PHYSICAL REVIEW B* 62.5 (2000).

[11] James F. Ziegler, M.D. Ziegler, and J.P. Biersack c. "SRIM – The stopping and range of ions in matter". In: *Nuclear Instruments and Methods in Physics Research B* 268 (2010).